

Research Paper

Alkbh4 and Atrn Act Maternally to Regulate Zebrafish Epiboly

Qingrui Sun*, Xingfeng Liu*, Bo Gong, Di Wu, Anming Meng, Shunji Jia✉

State Key Laboratory of Membrane biology, Tsinghua-Peking Center for Life Sciences, School of Life Sciences, Tsinghua University, Beijing 100084, China.

* These authors contributed equally to this work.

✉ Corresponding author: Shunji Jia, E-mail: jiasj@mail.tsinghua.edu.cn

© Ivyspring International Publisher. This is an open access article distributed under the terms of the Creative Commons Attribution (CC BY-NC) license (<https://creativecommons.org/licenses/by-nc/4.0/>). See <http://ivyspring.com/terms> for full terms and conditions.

Received: 2017.01.15; Accepted: 2017.07.11; Published: 2017.09.02

Abstract

During embryonic gastrulation, coordinated cell movements occur to bring cells to their correct position. Among them, epiboly produces the first distinct morphological changes, which is essential for the early development of zebrafish. Despite its fundamental importance, little is known to understand the underlying molecular mechanisms. By generating maternal mutant lines with CRISPR/Cas9 technology and using morpholino knockdown strategy, we showed that maternal *Alkbh4* depletion leads to severe epiboly defects in zebrafish. Immunofluorescence assays revealed that *Alkbh4* promotes zebrafish embryonic epiboly through regulating actomyosin contractile ring formation, which is composed of Actin and non-muscular myosin II (NMII). To further investigate this process, yeast two hybridization assay was performed and *Atrn* was identified as a binding partner of *Alkbh4*. Combining with the functional results of *Alkbh4*, we found that maternal *Atrn* plays a similar role in zebrafish embryonic morphogenesis by regulating actomyosin formation. On the molecular level, our data revealed that *Atrn* prefers to interact with the active form of *Alkbh4* and functions together with it to regulate the demethylation of Actin, the actomyosin formation, and subsequently the embryonic epiboly.

Key words: *alkbh4*, *atrn*, epiboly, actomyosin, Actin, NMII

Introduction

In early vertebrate development, embryos undergo a series of evolutionarily conserved cell movements, including epiboly, emboly and convergent extension. Epiboly in zebrafish begins at the late blastula stage, and results in tissue spreading and thinning until it encloses the entire yolk cell at the end of gastrulation [1, 2]. At this time, a zebrafish embryo has three distinct cellular layers: the enveloping layer (EVL), deep cell layer (DEL), and yolk cell that consists of the yolk syncytial layer (YSL) and yolk cytoplasmic layer (YCL). The EVL is a single-cell-thick layer that covers the DEL and contacts the YSL at its vegetal end [3]. During the progression phase of epiboly, contractile actomyosin ring, composed of Actin and non-muscular myosin II (NMII), in the E-YSL is regarded as the major force driving epiboly, which is achieved by pulling on the

EVL margin in the direction of the vegetal pole [2, 4-6]. However, the underlying molecular mechanism of actomyosin formation during epiboly remains to be elucidated.

Alkbh4 (alpha-ketoglutarate-dependent dioxygenase *alkB* homolog 4) belongs to the superfamily of Fe(II) and 2-oxoglutarate (2OG, alpha-ketoglutarate)-dependent dioxygenases, which can catalyze the demethylation of a variety of substrates [7]. Until now, nine mammalian *AlkB* homologs have been identified, *ALKBH1-8* and *FTO*. *ALKBH2* and *ALKBH3* possess DNA and/or RNA repair activity [8-10]. *ALKBH5* and *FTO* are two RNA demethylases that oxidatively remove the m6A (N6-methyladenosine) modification in mRNA [11, 12]. *ALKBH8* exhibits tRNA methyltransferase activity [13-15]. *ALKBH1* demethylates histone H2A K118 or K119

[16]. Recently, Li et al. reported that ALKBH4 functions to demethylate Actin at a mono methylated site (K84me1) and regulates actomyosin dynamics, and thereby the assembly of the contractile ring during mitosis [17]. Moreover, it is testified that Alkbh4 depletion in mice leads to spermatogenic defects and is lethal during early embryonic development [17, 18]. But it is unknown what role of Alkbh4 plays in zebrafish embryonic development.

Atrn (Attractin) is a member of CUB domain-containing protein family, which includes lots of cell adhesion and guidance proteins [19]. Previous reports show that there are two forms of ATRN proteins existing in both human and rat, a secreted form and a transmembrane form, as a result of alternative splicing. However, most of the species including zebrafish and mouse only express the transmembrane form of the ATRN protein [20, 21]. Secreted ATRN, an abundant serum glycoprotein, can function in monocyte/macrophage spreading and T cell clustering [19]. At the same time, secreted ATRN can promote glioma cell migration, implying ATRN is an important mediator of tumor invasiveness [22]. Transmembrane ATRN, a big single-pass transmembrane protein with about 1400 amino acids, plays important roles in monocyte function, pigmentation, neuronal degeneration and obesity [23-28]. As reported, transmembrane ATRN can act as a co-receptor for Agouti protein in MC1R and MC4R signaling pathway to regulate pigmentation and obesity [28, 29], as well as be involved in regulating the mitochondrial function [25]. However, nothing is known of Atrn functions during zebrafish embryonic development, especially in the epiboly process.

We show here for the first time that zebrafish maternal genes *alkbh4* and *atrn* are both critical for the embryo epibolic morphogenesis. They are both required for the formation of actomyosin in the E-YSL, and that in either of them absence, the major force driving epiboly is perturbed. Finally, we found that Atrn interacts with Alkbh4 and promotes the binding affinity between Actin and NMII, subsequently regulates the formation of actomyosin band in the E-YSL during zebrafish epibolic movement.

Materials and Methods

Zebrafish strains

Tuebingen strains of zebrafish were ethical approved by the Animal Care and Use Committee of Tsinghua University. Zebrafish embryos were obtained from natural mating and were cultured in Holtfreter solution at 28.5°C. Developmental stages of embryos were determined according to Kimmel et

al [30].

Constructs

alkbh4-5'UTR-GFP plasmid was generated by inserting a part of 5'UTR and coding sequence of *alkbh4* into pEGFP-N3 (Clontech) with the forward primer 5'-GGAATTCAGGTCCTTTGAGTCTCTGCTAATGAGC-3' and the reverse primer 5'-CGGGATCCACAACCTGGATTCATCATCAGAGC-3'. For constructing *atrn*-5'UTR-GFP plasmid, a DNA fragment including *atrn*-MO targeting sites was inserted into the pEGFP-N3 vector, the sequences were as follows: 5'-GCGGGCCCGGGATCCCTGTTTGTGCGCGAATGGCTGCGGAGGGATCCATCGCCACC-3'.

For genes' expression, *alkbh4* and *atrn* coding sequences were amplified and ligated to pCS2-Flag and pCS2-HA vectors respectively. For pCS2-Flag-Alkbh4-Mut, H169A/D171A sites mutation primers were as follows: 5'-GAGCGGGGCTCTGCCATTGACCCCGCACTGGCTGACGCTGGCTGTGGGGGGAGCGGC-3' (forward); 5'-GCCGCTCCCCCACAGCCAGGCGTCAGCCAGTGCAGGGTCAATGGCAGAGCCCCGCTC-3' (reverse). For generating *actin*, *actin-K84A* and *actin-K84R* mRNA constructs, the following primers were used: 5'-GGAATTCACCATGGATGAGGAAATCGCTGCCCTGGTC-3' (*actin-F*); 5'-CGCTCGAGCCGCCACCTCCGAAGCACTTCTGTGAACGATGGATGGGC-3' (*actin-R*); 5'-GACCAA CTGGGATGACATGGAGGCCATCTGGCATCACA CTTTCTACAATGAGC-3' (*actinK84A-midF*); 5'-GCTCATTGTAGAAGGTGTGATGCCAGATGGCCTCCATGTCATCCCAGTTGGTC-3' (*actinK84A-midR*); 5'-GACCAA CTGGGATGACATGGAGAGGATCTGGCATCACA CTTTCTACAATGAGC-3' (*actinK84R-midF*); 5'-GCTCATTGTAGAAGGTGTGATGCCAGATCCCTCCATGTCATCCCAGTTGGTC-3' (*actinK84R-midR*).

Whole-mount *in situ* hybridization (WISH)

Digoxigenin-UTP-labeled antisense RNA probes were synthesized *in vitro* using a linearized plasmid or PCR product as template. The templates for *dlx3b* and *ntla* were linearized as previously reported [31], while those for *alkbh4*, *atrn*, *mpi* and *ranbp10* were amplified with the following primers:

alkbh4:

5'-CTCCAGAAGAATGATCTGATTC-3'

(forward) and

5'-TAATACGACTCACTATAGGGCACTTTACATTTGTGCAATTGAAC-3' (reverse);

atrn:

5'-GTGGCATTGGAGACGGACGAGGAGC-3'

(forward) and

5'-TAATACGACTCACTATAGGGCAGTTAGC

GCACCAAACATGCACAC-3' (reverse);

mpi:

5'-TCTGTCCGGAGACTGTGTGGAGTGTATG
GC-3' (forward) and

5'-TAATACGACTCACTATAGGGGAAGCGTC
TCCTACAGTAAGCAGCAGCTC-3' (reverse);

ranbp10:

5'-CTCATTGACAGCACAGGCGCAGACA
GTC-3' (forward) and

5'-TAATACGACTCACTATAGGGGCTTCTGG
CAAGCGGCACACCAATTC-3' (reverse).

Whole-mount *in situ* hybridization was performed as previously described [31]. Embryos after whole-mount *in situ* hybridization were immersed in glycerol and photographed using the Ds-Ri1 CCD camera under a Nikon SMZ1500 stereoscope.

Semi-quantitative PCR

Zebrafish cDNA at indicated stages were prepared by reversely transcribed enzyme M-MLV reverse transcriptase (Promega). For *alkbh4* PCR, the primer pairs were as follows: 5'-ATGATGCTTTTTCGCTACTGTGAC-3' and 5'-CCGCTCGAGTATAGAGCACCCTGGAAGCTC-3'. For *atrn* PCR, the primer pairs were as follows: 5'-GCACACAGGTGAGGTAGAAGAGTTC-3' and 5'-GATATCAGATCTCTCGAGGAATTCCTACTGCCAGACTGACTGTCC-3'. For β -actin PCR, the primer pairs were as follows: 5'-ATGGATGATGAAATTGCCGCAC-3' and 5'-ACCATCACCAGAGTCCATCACG-3'. Relative *alkbh4* and *atrn* mRNA levels are measured by ratio of *alkbh4* or *atrn* band intensity to that of β -actin band.

Morpholinos and microinjection

The morpholino oligonucleotides (MOs) were synthesized by Gene Tools, LLC, and the sequences were as follows: *alkbh4*-MO1, 5'-ACACCTCATTTA GATCATCAGCTCA-3'; *alkbh4*-MO2, 5'-AAGTAG GCAAAAAGCACCACAAGCA-3'; *atrn*-MO, 5'-TC CGCAGCCATTCGCGCACAAACAG-3'; *std*-MO, 5'-CCTCTTACCTCAGTTACAATTTATA-3'. MPPI-2 quantitative injection equipment (Applied Scientific Instrumentation Co.) was used for microinjection. About 1 nl morpholino solution was injected into the yolk of each embryo at 1-cell stage. The injection dose was the amount of a morpholino received by a single embryo.

Generation of mutant lines with CRISPR/Cas9

gRNAs for making *alkbh4* and *atrn* mutant lines were designed to target the third exon of *alkbh4* and second exon of *atrn* respectively. Their target sequences were as follows: 5'-CCATGTGGGAA GCTTCAGCGGCC-3' (*alkbh4*) and 5'-GGCTACCTCT

CTGATGGACCAGG-3' (*atrn*). According to previous work, 100 pg gRNA with 300 pg Cas9 mRNA was co-injected into one-cell stage embryos. PCR primer pairs for identifying *alkbh4* mutant embryos were 5'-CATGAGACATCTGTCTATCCAAAGGAC-3' and 5'-TAGAGGAGCACCCCTGGAAGC-3'; while for *atrn* mutant embryos were 5'-CACTCTGTGCTTGTG GTTTC-3' and 5'-CGATACTGGTATTGGTGCAT CTC-3'. Then the PCR products were cut by T7 Endonuclease I firstly and then sequenced to identify their genotypes.

Whole-mount Immunofluorescence

Zebrafish embryos at indicated stages were fixed by 4% paraformaldehyde at 4°C and washed by PBST (0.1% Triton X-100) for 3 times. Then the embryos were incubated in PBST (0.5% Triton X-100) for 1 hr at RT and washed by PBST (0.1% Triton X-100) for 3 times, followed by blocking in block buffer (10% normal goat serum, 2% BSA, 1% DMSO, 0.1% Triton X-100 in PBS) for 2 hrs. Thereafter, phalloidin and/or primary antibodies in block buffer were added overnight at 4°C, and then secondary antibodies were used for another 5 hrs at RT. The following primary antibodies and dilutions were used: mouse anti-NMII with 1:100 dilution (ab55456, Abcam), mouse anti-HA with 1:100 dilution (sc-7392, Santa Cruz), rabbit anti-GFP with 1:100 dilution (ab290, Abcam). Embryos were imaged by Zeiss LSM 710 confocal microscope.

Yeast two hybridization assay

Zebrafish *alkbh4* was cloned into pGBKT7 vector and used for bait. The cDNA library was derived from a mixture of zebrafish embryos at 1-cell, 40% epiboly, 5-somite and 24 hpf stages, and was described in our previous study [32, 33]. For a detailed description of the protocol, please refer to Matchmaker Two-Hybrid System 3 & Libraries User Manual from Clontech.

Immunoprecipitation and Western blot

Immunoprecipitation and Western blot experiments were performed as previously described [32, 33]. For *Alkbh4* and *Atrn* interaction, Flag-*alkbh4*/*alkbh4*-mut and HA-*atrn* were transiently expressed in HEK293T cells. Cells were collected and lysed after 40 hrs transfection. For endogenous Actin and NMII interaction, wild-type zebrafish embryos were collected at 75% epiboly stage, while the *MZalkbh4* and *MZatrn* mutant embryos were collected at similar morphological stages. Embryonic yolk was first removed by pipetting repeatedly with 200 μ l tips, and then the embryonic cells were collected by centrifuge and lysed in TNE buffer. Mouse anti-Flag (1:1000; F1804,

Sigma), mouse anti-NMII (1:100 for IP and 1:1000 for WB; ab55456, Abcam), goat anti-Actin (1:2000; sc-1615, Santa Cruz), mouse anti- α -Tubulin (1:100; T6199, Sigma) and rabbit anti-phospho-Histone H3 (Ser10) (1:100; #9701, CST) antibodies were used.

Measurements and Statistical analysis

The epiboly percentage, body length, actomyosin band width, cell length and cell width were all measured by Image J software. All the data were averaged from three times of independent experiments at least, and expressed as mean plus s.d. Student's T-tests (two-tailed, unequal variance) were used to determine p-values, and *, $p < 0.01$ indicated the significance levels.

Rhodamine B isothiocyanate-Dextran endocytosis assay

The dechronized embryos at 50% and 75% epiboly stages were incubated in Rhodamine B isothiocyanate-Dextran solution (Sigma, R8881) at 10 mg/ml in holfreter water for 30 minutes [5]. After washing 2 times, embryos were imaged by Zeiss LSM 710 confocal microscope.

Results

The spatio-temporal expression of *alkbh4* in zebrafish development

The earliest stages of embryonic development rely on maternal genes [34]. However, this maternal regulation has been little studied in vertebrates, owing to the difficulty in manipulating maternal gene function. With the development of CRISPR/Cas9-mediated genome engineering, it becomes convenient to generate mutant embryos for specific genes, and therefore identify their maternal effects. In our previous work, we carried out RNA-seq analysis to detect maternally enriched genes in zebrafish early development. It was found that *alkbh4* mRNA level was extremely much higher than other *alkbh* family members, especially in the oocytes (Figure 1A). The zebrafish *alkbh4* has an ORF that encodes a peptide of 268 amino acids and exhibits 48.3%, 49.2%, and 50.3% identities in amino acid sequence with mouse, rat and human ALKBH4 respectively (Figure 1B). Being interested in its functions in the embryonic early development, we first examined its expression pattern by whole-mount *in situ* hybridization with digoxin-labeled antisense probe. It was shown that *alkbh4* mRNA is present in fertilized eggs, suggesting that it is maternally distributed. From the 2-cell stage to dome stage,

alkbh4 mRNA can be continuously detected in all blastodermal cells (Figure 1C). Notably, *alkbh4* maternal mRNA decreases gradually and becomes almost undetectable after dome stage with *in situ* hybridization. At 24 hrs postfertilization (hpf), its zygotic mRNA was determined to emerge in the forebrain, midbrain and otic vesicles (Figure 1C). Using β -actin as an internal control, semi-quantitative RT-PCR for comparison of *alkbh4* mRNA expression level at different stages was carried out (Figure 1D). The statistical data demonstrated that expression of maternal *alkbh4* mRNA decreased quickly during the very early stage of embryogenesis (Figure 1E), which raising the possibility that Alkbh4 might be an important maternal factor to regulate zebrafish early embryonic development.

Alkbh4 depletion affects epibolic morphogenesis

In order to investigate the functions of endogenous *alkbh4* in zebrafish embryonic development, we synthesized two specific antisense morpholino oligonucleotides (MO), *alkbh4*-MO1 and *alkbh4*-MO2, which target different sequences in the 5' untranslated region (5' UTR) of *alkbh4*, to block its translation. Co-injection of 10 ng *alkbh4*-MO1 or *alkbh4*-MO2 with *alkbh4*-5'UTR-GFP reporter plasmid, which encodes a fusion Alkbh4-GFP protein, showed that both morpholinos could effectively block the translation of *alkbh4* mRNA, and *alkbh4*-MO2 was more effective (Figure 2A). Compared to the embryos injected with standard MO (std-MO), those injected with *alkbh4*-MO1 or *alkbh4*-MO2 alone displayed slower epiboly in a dose-dependent manner (Figure 2B). At the same time, we noticed that the epiboly defects caused by injection of *alkbh4*-MO2 was much severe than that of *alkbh4*-MO1, which was consistent with their efficacy as shown in Figure 2A. Close examinations at higher magnifications also revealed that the cell movements in EVL, DEL and YSL were all slower in the morphant embryos (Figure 2B, last panel). When most of the std-MO injected embryos developed to 30% epiboly stage (5 hpf), embryos injected with 10 ng *alkbh4*-MO2 almost didn't initiate the epiboly process (Figure 2B and 2C). While at 80% epiboly stage (8 hpf), the embryos injected with 10 ng *alkbh4*-MO2 only reached about 60% epiboly on average ($n=64$) (Figure 2B and 2D). Therefore, it is possible that the observed epibolic defects might be due to the requirement of *alkbh4* for cell motility during zebrafish embryonic development.

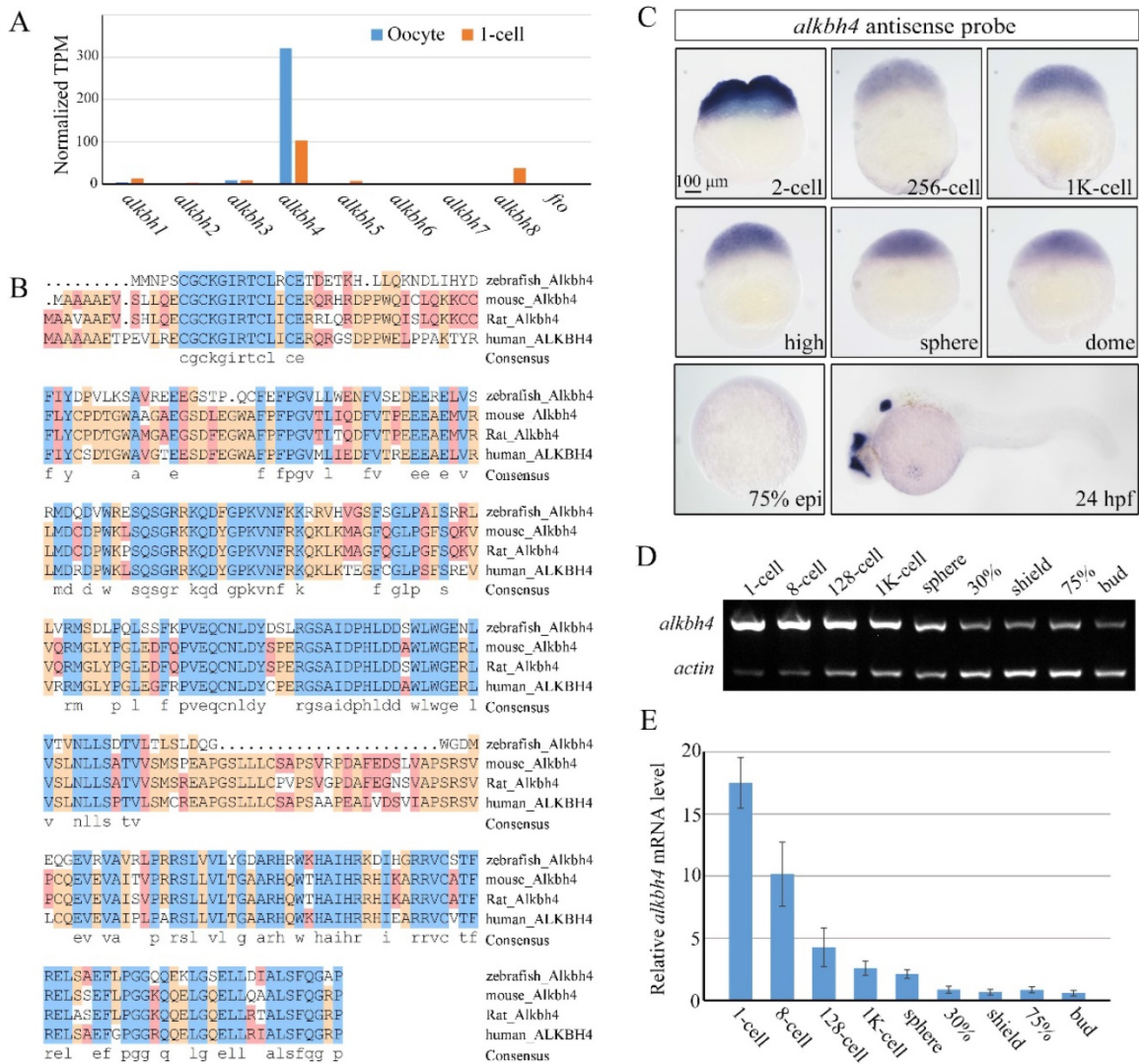


Figure 1. Spatiotemporal expression pattern of *alkbh4* in zebrafish embryos. (A) mRNA levels of *alkbh* family members in zebrafish oocyte and 1-cell embryo from RNA-seq data. Normalized transcripts number per million of *alkbh1-8* and *fto* transcripts are shown. **(B)** Protein sequences alignment of Alkbh4 among different species. **(C)** *alkbh4* mRNA expression pattern in wild-type zebrafish embryos were detected by whole-mount *in situ* hybridization at indicated stages. **(D, E)** Semi-quantitative RT-PCR detection of zebrafish *alkbh4* mRNA level at indicated stages. The relative expression ratio was calculated from the band intensity between *alkbh4* and β -actin (internal control). Scale bars: 100 μm in (C).

To further validate and distinguish the functions of maternal mRNA and zygotic mRNA of *alkbh4* in embryonic epiboly process respectively, we generated corresponding maternal and zygotic mutants using the CRISPR/Cas9-mediated approach [35]. By targeting the third exon of the *alkbh4* gene, we obtained three kinds of deletion mutations, including *alkbh4*^{cd4} with -5/+1 bp alteration, *alkbh4*^{cd8} with 8 bp deletion, and *alkbh4*^{cd20} with 20 bp deletion, all of which led to a premature stop codon and therefore the lack of the catalytic domain of the protein (Figure 3A). An initial observation indicated that the zygotic *alkbh4*^{cd4/cd4}, *alkbh4*^{cd8/cd8}, and *alkbh4*^{cd20/cd20} homozygous mutants appeared normally without obvious morphological defects during embryogenesis (Figure 3B and data not shown). Then these *Zalkbh4* mutant embryos were raised to adulthood, thus

allowing generating maternal *Malkbh4* mutant embryos by outcrossing female homozygous to the male wild-type fish, and then obtaining the maternal-zygotic *MZalkbh4* mutants by intercrossing homozygous fish directly. Our results indicated that embryonic epiboly initiation and progression were significantly delayed in *Malkbh4*^{cd4/cd4} and *MZalkbh4*^{cd4/cd4} mutant embryos, although there was no obvious defect in *Zalkbh4*^{cd4/cd4} mutant (Figure 3B-3D). Because the three different lines of *Malkbh4* and *MZalkbh4* mutants have similar phenotype (data not shown), we only focused on *MZalkbh4*^{cd4/cd4} mutation in subsequent analyses. Consistently, the morphological defects of mutant embryos were quite similar to those of *alkbh4* morphant embryos (Figure 2B-2D). To examine the exact marginal positions of EVL and deep cells in *MZalkbh4* mutant embryos, we

performed phalloidin and DAPI staining. Our analyses indicated that, compared with control embryos, movements of EVL and deep cells to the vegetal pole were largely postponed in the mutant embryos (Supplementary Figure S1A). To validate the lack of wild-type *alkbh4* mRNA transcripts in the MZ*alkbh4*^{cd4/cd4} mutant embryos, we performed whole *in situ* hybridization at 2-cell and 24 hpf stages, following with genotyping using the same *in situ* hybridized embryos. Our results showed that *alkbh4* mRNA was almost disappeared in MZ*alkbh4* mutant embryos at both 2-cell and 24 hpf stages, meanwhile *alkbh4* mutant mRNA was also undetectable probably due to the nonsense-mediated mRNA decay (Figure 3E). Taking into account that embryonic epiboly was only significantly delayed in maternal, but not zygotic *alkbh4* depleted embryos, we claimed that the contribution of *alkbh4* to gastrulation cell epibolic

movements is a strictly maternal-effect.

Besides epiboly, we also paid attention to the convergent extension (CE) movement in both MZ*alkbh4* and *Malkbh4* mutants. To investigate whether the CE movements are affected or not, we examined the expression of two marker genes, the midline marker *ntla* and the neural plate boundary marker *dlx3b* in mutant embryos [31]. Due to the existence of epiboly delay in mutant embryos, we focused on comparing the results at morphologically comparable stage, but not at the same time point. We found that at bud stage, *alkbh4* depletion resulted in wider neural plate (marked by *dlx3*) and notochord (marked by *ntla*) in 93% (n=45) of MZ*alkbh4* and 91% (n=35) of *Malkbh4* mutant embryos (Figure 3F). These observations further support the notion that *alkbh4* participates in CE movements during zebrafish embryogenesis.

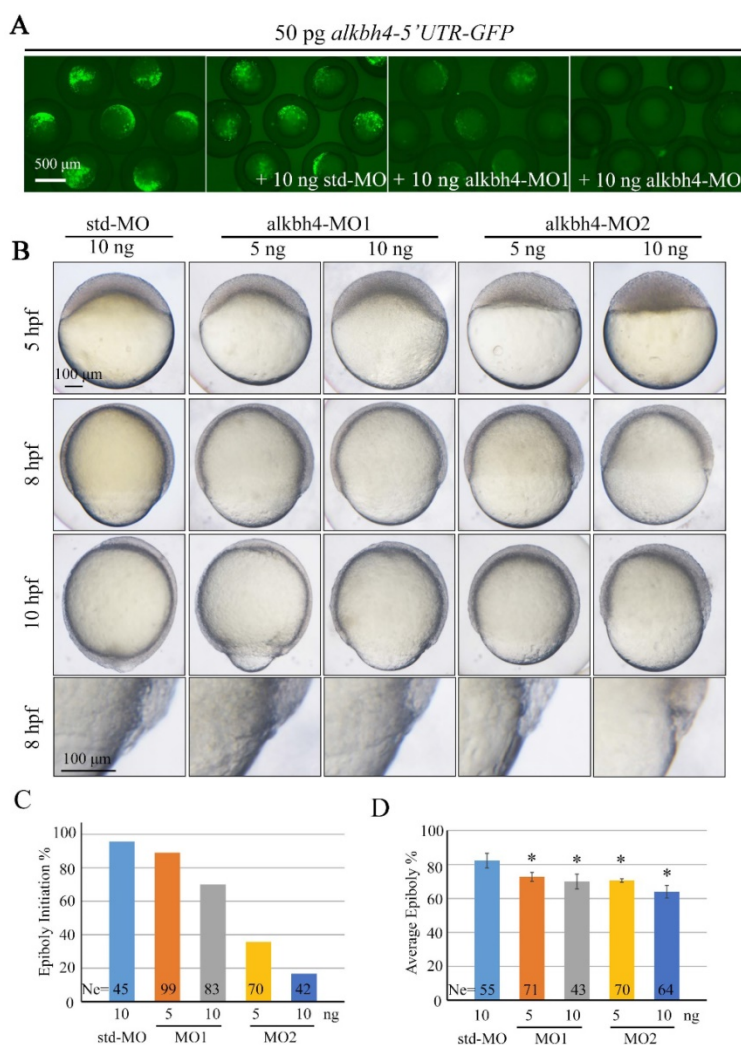


Figure 2. Morpholino knockdown of *alkbh4* leads to epiboly initiation and progression delays. (A) Effectiveness of *alkbh4* morpholinos. 50 pg *alkbh4*-5'UTR-GFP plasmid DNA was injected alone or with 10 ng std-MO, *alkbh4*-MO1 or *alkbh4*-MO2 at 1-cell stage. The injected embryos were observed for GFP expression at late gastrulation stages. (B) Morpholino knockdown of *alkbh4* leads to epiboly delay in a dose dependent manner. Embryos were observed and photographed at indicated stages. Magnified observations of the embryonic marginal cell layers are shown at the last panel. (C) Epiboly initiation in (B) was measured by the percentage of embryos with yolk cell doming at 5 hpf. (D) Epiboly progression in (B) was measured by the average epiboly percentage of the embryos at 8 hpf. Ne, the number of observed embryos. *, p<0.01. Scale bars: 500 μm in (A); 100 μm in (B).

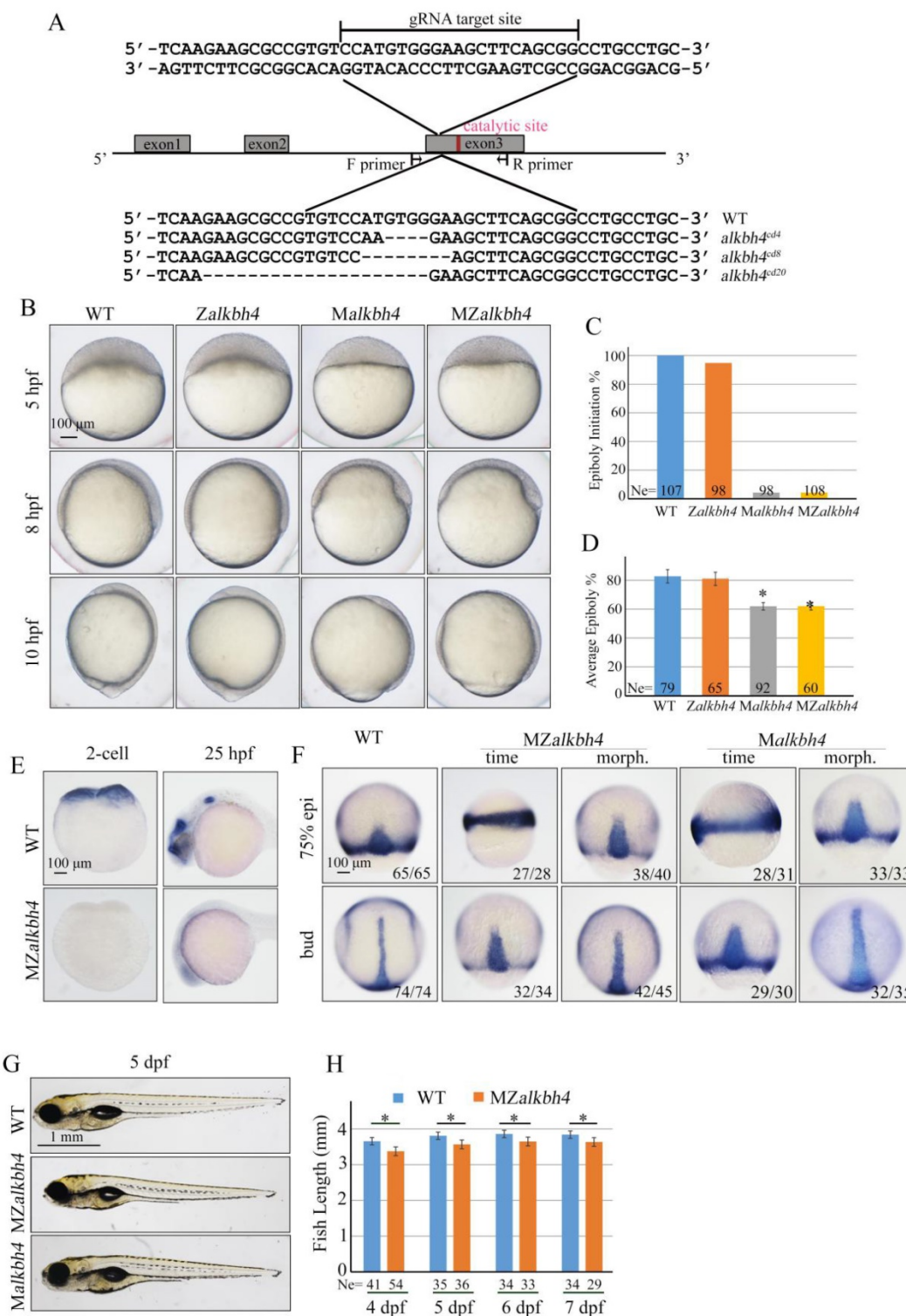


Figure 3. Maternal *alkbh4* mutation leads to epiboly delay. (A) CRISPR/Cas9-mediated deletion of *alkbh4*. Zebrafish *alkbh4* contains 3 exons, and gRNA was designed to target the third exon. A specific genomic region was amplified from F₂ individual embryo and sent for sequencing. The sequencing results of target sites are shown below, including the wild-type form and three kinds of *alkbh4* mutant forms. (B) Maternal but not zygotic *alkbh4* mutation results in epiboly initiation and progression delays. Wild-type, *Zalkbh4*, *Malkbh4* and *MZalkbh4* mutant embryos were collected after fertilization at the same time and then imaged at the indicated time points. (C) Epiboly initiation in (B) was measured by the percentage of embryos with yolk cell doming at 5 hpf. (D) Epiboly progression in (B) was measured by the average epiboly percentage of the embryos at 8 hpf. (E) *In situ* hybridization results of *alkbh4* mRNA expression in wild-type and *MZalkbh4* embryos at 2-cell and 25 hpf stages are shown. (F) CE movements are defective in *MZalkbh4* and *Malkbh4* mutant embryos. The mutant embryos were collected not only at the same time point but also at the morphologically comparable stages compared with wild-type embryos. *dlx3b* and *ntla* probes were used simultaneously for *in situ* hybridization. The ratios of embryos with representative pattern are indicated at the right corner of each picture. (G) The body length decreases in *MZalkbh4* and *Malkbh4* mutant larvae. Representative pictures of wild-type and mutant larvae at 5 dpf are shown. (H) The body lengths of wild-type and *MZalkbh4* mutant larvae at 4 dpf, 5 dpf, 6 dpf and 7 dpf were measured by Image J software. The statistical results are shown here. Ne, the number of observed embryos. *, p<0.01. Scale bars: 100 μm in (B, E, F); 1 mm in (G).

Taken together, these data suggest that maternally, but not zygotically expressed *alkbh4* is critical for embryonic epiboly and CE movements during gastrulation. Additionally, we found that the average body lengths of *MZalkbh4* and *Malkbh4* mutants were reduced obviously compared with those of wild-type larvae in corresponding stages (Figure 3G, 3H, and data not shown), suggesting the maternal effect of *alkbh4* can last to larval stages.

***alkbh4* is required for Actin and NMII recruitment in the E-YSL and EVL cell-shape changes**

Previous analyses indicated that during epiboly of the zebrafish embryo, the actomyosin ring, composed of Actin and NMII, within the yolk cytoplasm along the margin of the EVL is critical for the EVL marginal cells constriction, and subsequently the movement of the EVL over the yolk cell surface [6, 36]. In order to address whether the formation of actomyosin within the E-YSL is affected in *MZalkbh4* mutant embryos or not, we first stained the embryos with fluorescent labeled phalloidin and observed by confocal fluorescent microscopy. Our data showed

that at 75% epiboly, Actin became enriched at the EVL-YSL interface in wild-type embryos, and the average width of the band was 14.4 μm (n=32) approximately (Figure 4A and 4B). However, only a relatively thin band of Actin with an average width of 7.0 μm (n=20) was detected in *MZalkbh4* mutant embryos at the same time point (Figure 4A and 4B). Even when the mutant embryos developed to the morphologically comparable stage, the staining of Actin was still distinctly thinner (6.2 μm , n=24) than the wild-type embryos (Figure 4A and 4B). Similarly, the expression of NMII was also examined by its specific antibody against NMII heavy chain. At 75% epiboly, the average width of NMII declined from 13.1 μm (n=20) in wild-type embryos to 6.1 μm (n=20) at the same time point and 5.3 μm (n=19) at the same morphologically comparable stage in *MZalkbh4* mutant embryos respectively (Figure 4A and 4B). After confirming the similar results in *Malkbh4* mutant embryos (Supplementary Figure S2A and S2B), we concluded that the formation of actomyosin ring was largely inhibited in maternal *alkbh4* depleted embryos.

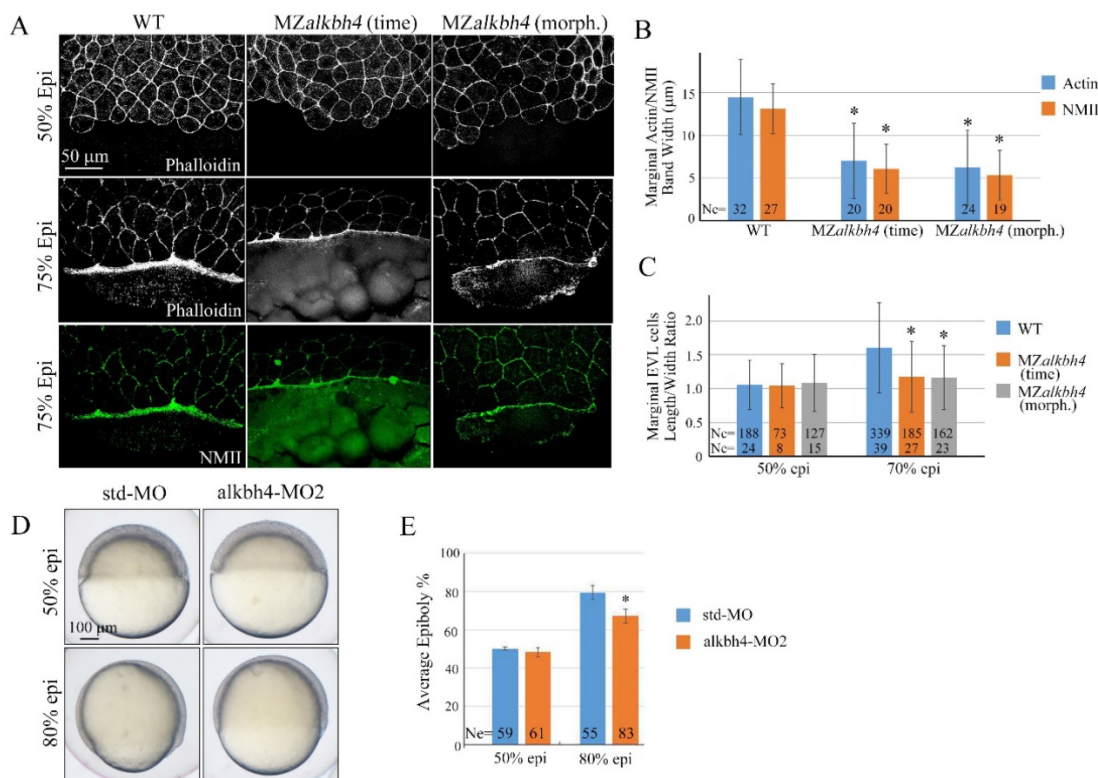


Figure 4. *alkbh4* regulates actomyosin band formation in *MZalkbh4* embryos. (A) Confocal images of phalloidin stained embryos at 50% epiboly, and phalloidin and anti-NMII double stained embryos at 75% epiboly. phalloidin and anti-NMII co-staining showing the defects of actomyosin band formation and marginal EVL cells morphology in *MZalkbh4* embryos. The mutant embryos were collected not only at the same time point but also at the morphologically comparable stages compared with wild-type embryos. Embryos were laterally viewed with animal pole to the top and vegetal pole to the bottom. (B) Quantitative measurements of actomyosin band widths in (A) at 75% epiboly stage, which were represented by the widths of Actin and NMII staining in the E-YSL separately. (C) Quantitative measurements of the marginal EVL cell length/width ratios in (A) at both 50% and 75% epiboly. Ne, the number of observed embryos; Nc, the number of observed cells. *, p<0.01. (D) Epiboly defects caused by YSL-injection of *alkbh4*-MO2. At 4 hpf, 10 ng std-MO and *alkbh4*-MO2 were injected into the yolk cell of embryos and epiboly progression were observed at 50% and 80% epiboly stages. (E) Epiboly progression in (D) was measured by the average epiboly percentage of the embryos. Ne, the number of observed embryos. *, p<0.01. Scale bars: 50 μm in (A); 100 μm in (D).

Given the evidence that the contractile actomyosin ring within the E-YSL drives the late phase of epiboly, possibly through coordinated EVL marginal cell shape changes [5, 6, 36], we analyzed MZ*alkbh4* and *Malkbh4* mutant embryos at 50% and 75% epiboly stages by phalloidin staining. As shown in Figure 4A and Supplementary Figure S2A, at 50% epiboly stage, marginal cells of wild-type, MZ*alkbh4* and *Malkbh4* mutant embryos were typically oval shaped. Thereafter, at 75% epiboly stage, the staining results revealed a delay of the elongation of the marginal EVL cells along the animal-vegetal axis in MZ*alkbh4* and *Malkbh4* mutant embryos. To quantitatively compare the differences in EVL marginal cell constriction between wild-type and mutant embryos, the length to width ratios of individual border cells for about 10 cells per embryo were measured. Compared to the wild-type embryo, no significant difference of this ratio at 50% epiboly, but a remarkable declining at 75% epiboly was detected in both mutant embryos (Figure 4C and Supplementary Figure S2C), revealing a delay in the coordinated EVL marginal cell shape changes in the absence of maternal *alkbh4*. Taken together, it is indicated that *alkbh4* is involved in the formation of actomyosin ring within the E-YSL and therefore regulates the epibolic morphogenesis in zebrafish.

To directly address the role of *alkbh4* in the YSL, we injected its morpholino into this tissue at 4 hpf as described by Mathias Köppen et al [6]. Embryos injected with 10 ng *alkbh4*-MO2 displayed no obvious defect until 50% epiboly (Figure 4D). However, when the control group developed to 80% epiboly, the embryos injected with *alkbh4*-MO2 only reached about 67% epiboly on average (n=83), meanwhile showing a delay in epiboly of the DEL and the EVL cells (Figure 4D and 4E). Therefore, it is indicated that *alkbh4* plays a direct role in the E-YSL to regulate cell mobility.

Alkbh4 associates and co-localizes with Atrn

Protein-protein interactions play fundamental roles in many biological processes. In order to better understand how *Alkbh4* activity is regulated in embryonic epiboly process, we devised a comprehensive yeast two-hybrid screen using *Alkbh4* as the bait protein to look for *Alkbh4*-binding partners expressed in zebrafish embryos. By screening library, several proteins, such as *Atrn*, *Ranbp10* and *Mpi*, were identified as the partners of *Alkbh4* (data not shown). What draws more of our attention is that the spatio-temporal expression of *atrn* is quite similar to *alkbh4*, while the other two genes are not (Figure 5A). To confirm that there is a real physical association between *Alkbh4* and *Atrn*, we carried out a

coimmunoprecipitation (Co-IP) experiment. As shown in Figure 5B, immunoprecipitation of HA-tagged *Atrn* in HEK293T cells indeed retrieved Flag-tagged human *ALKBH4*, implying an existing interaction between them. Additionally, to reveal the subcellular localization of *Atrn* and *ALKBH4* proteins, we injected HA-tagged *atrn* plasmid DNA and GFP-tagged *ALKBH4* mRNA into one cell at 4-cell stage of zebrafish wild-type embryos, and then detected their expression by immunofluorescence. We found that overexpressed HA-*Atrn* was well co-localized with *ALKBH4*-GFP in zebrafish embryonic cells, where they were distributed throughout the cells with prominent cytoplasmic and plasma membrane localization (Figure 5C), also supporting a possible interaction between them.

***atrn* plays a similar role to *alkbh4* in epibolic morphogenesis**

Different from human and rat, zebrafish *atrn* gene only encodes the transmembrane form of the protein with 1,345 amino acids, as in the case of mouse. Zebrafish *Atrn* protein has 68.04%, 67.55%, and 67.67% identities with human, rat and mouse transmembrane form of *Atrn*. We first examined the expression pattern of zebrafish *atrn* in detail and found that it was extremely similar to that of *alkbh4*. The results showed that *atrn* mRNA is maternally distributed and continuously exists in all blastodermal cells until dome stage (Figure 6A). Then, *atrn* maternal mRNA decreases and its zygotic mRNA appears in the forebrain, midbrain and otic vesicles at 24 hpf (Figure 6A). Semi-quantitative RT-PCR was also carried out to confirm the expression level of *atrn* during early developmental stages, showing that the expression of maternal *atrn* mRNA decreased obviously after dome stage (Figure 6B and 6C).

In order to explore functions of *Atrn* in embryonic development, we synthesized *atrn*-MO, which targeted the 5'UTR region of *atrn* mRNA, to block its translation. We first confirmed the efficacy of *atrn*-MO by its ability to block the expression of the corresponding 5'UTR-GFP reporter construct (Figure 6D). Compared to std-MO, *atrn*-MO injected embryos displayed slower epiboly in a dose dependent manner, which was quite similar to the defects of *alkbh4* morphant or mutant embryos (Figure 6E, 2B and 3B). A large number of statistical results showed that when most of embryos injected with std-MO developed to 30% epiboly stage (5 hpf), about 20% (n=72) embryos injected with 10 ng *atrn*-MO did not initiate the epiboly process (Figure 6F). While at 80% epiboly stage (8 hpf), the embryos injected with 10 ng *atrn*-MO only reached about 60% epiboly on average (n=50) (Figure 6G). Thus, it is suggested that *atrn*

might be involved in regulating the epiboly process of zebrafish embryos.

To substantiate the phenotype of *atrn* morphant is true, we generated its mutants using the CRISPR/Cas9 technology. By targeting second exon of *atrn*, two kinds of deletion mutants, *atrn^{cd4}* and *atrn^{cd5}* were obtained, both of which were lack of C-terminal part of the protein (Figure 7A). After confirming that both zygotic *atrn^{cd4/cd4}* and *atrn^{cd5/cd5}* homozygous mutants developed normally without obvious morphological defect during embryogenesis (Figure 7B and data not shown), these *Zatrn* mutants were raised to adulthood to generate *Matrn* and *MZatrn* mutant embryos. Similar to *atrn* morphants, embryonic epiboly initiation and progression were significantly delayed in *Matrn* and *MZatrn* mutants (Figure 7B-7D), which is also extremely similar to the defects of *alkbh4* morphant and mutant embryos (Figure 3B-3D), suggesting that the maternally expressed *atrn* is important for embryonic epiboly process. Additionally, we examined the CE movements in *MZatrn* and found that although the *ntla/dlx3b* expression pattern of mutant embryos looked very different from that of wild-type embryos at the same time point after fertilization (9 hpf), but they finally became similar at the same morphological stage (90% epiboly) (Figure 7E). Therefore, it is suggested that *atrn* has little effect on the CE movements of gastrulation, which is different from

alkbh4 (Figure 3F). Taken together, these data suggest that the maternal but not zygotic *atrn* is critical for embryonic epiboly during gastrulation.

***atrn* regulates actomyosin formation and EVL cell-shape changes**

Because *Alkbh4* was found to regulate actomyosin ring formation during embryonic epiboly, we wondered whether the Actin and NMII accumulation within the E-YSL is also affected in *MZatrn* mutant embryos or not. The phalloidin and NMII immunostaining results showed that compared to wild-type embryos at 75% epiboly, the accumulation of Actin and NMII within the E-YSL were inhibited obviously in *MZatrn* mutant embryos, not only at the same time point but also at the morphologically comparable stage (Figure 8A). The corresponding statistical data were obtained and shown in Figure 8B. Besides that, we also analyzed the changes in EVL cell shape in phalloidin-stained embryos, and found that the length to width average ratio of marginal cells in *MZatrn* mutant decreased significantly, which was consistent with the defects of actomyosin-based contractility in the mutant embryos (Figure 8A and 8C). Similarly, we performed morpholino YSL-injection assays to demonstrate that *atrn* acts directly on the mobility of EVL cells and DEL cells to affect zebrafish epibolic morphogenesis (Figure 8D and 8E).

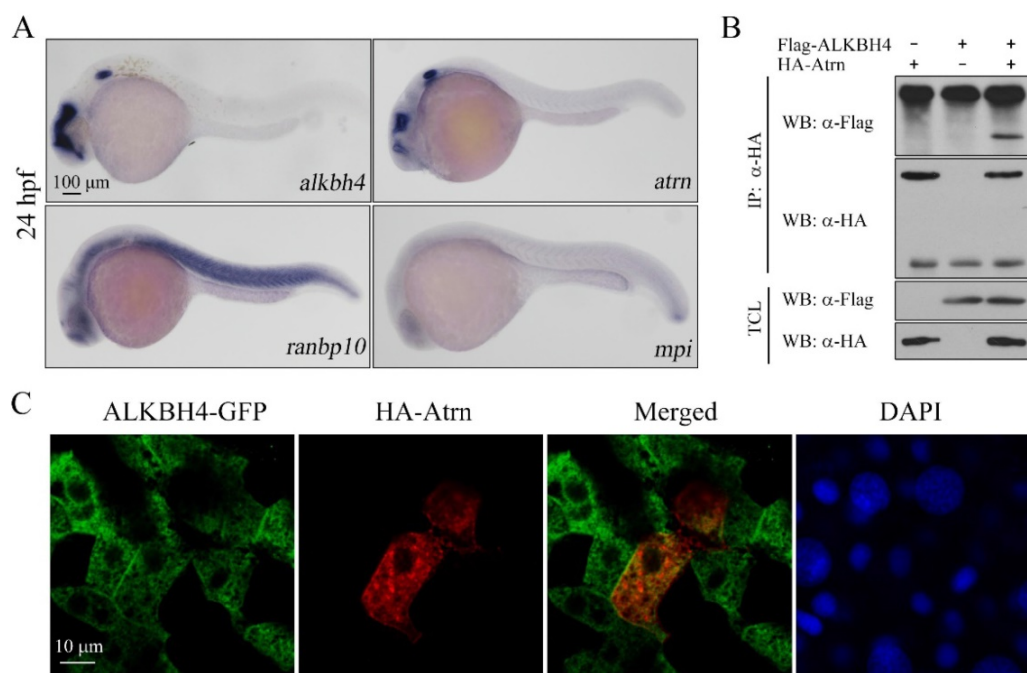


Figure 5. *Alkbh4* associates and co-localizes with *Atrn*. (A) Whole-mount *in situ* hybridization results of putative *Alkbh4* binding partners, including *atrn*, *ranbp10* and *mpi*. Only the expression pattern of *atrn* is similar to that of *alkbh4* at 24 hpf. (B) Flag-ALKBH4 was co-expressed with HA-Atrn in HEK293T cells and their interaction was examined by immunoprecipitation. HA-Atrn was immunoprecipitated with anti-HA antibody and the precipitates were examined by western blotting for the presence of ALKBH4 with anti-Flag antibody. TCL, total cell lysate. (C) Co-localization of ALKBH4-GFP with HA-Atrn in zebrafish embryonic cells. HA-Atrn plasmid DNA and ALKBH4-GFP mRNA were injected into one cell at 4-cell stage of the embryos. Embryos were double stained with corresponding antibodies at 75% epiboly stage. Scale bars: 100 μm in (A); 10 μm in (C).

Alkbh4 and Atrn regulate the actomyosin formation by regulating the Actin demethylation

So far, we thought that *alkbh4* and *atrn* might function together to regulate the formation of actomyosin, and subsequently the epiboly process in zebrafish early development. Given the evidences that Alkbh4 acts as an Actin demethylase to promote Actin-NMII interaction by erasing Actin K84 mono methylation [17], we constructed a catalytically inactive form of Alkbh4 (Alkbh4-Mut) with its catalytic domain mutated (H169A/D171A). We found that compared to the wild-type form of Alkbh4 (Alkbh4-WT), the catalytically inactive form of Alkbh4 (Alkbh4-Mut) showed a much lower affinity to interact with Atrn (Figure 8F). These data implied that Atrn might be involved in the catalytic function of Alkbh4. To validate our speculation and better understand the functional interplay between Alkbh4 and Atrn, we tested whether depletion of *atrn* would affect Actin-NMII interaction. Consistent with the fact that Alkbh4 regulates Actin-NMII interaction in

mammalian cells, it was demonstrated *in vivo* that Actin-NMII interaction was also disrupted in MZ*atrn* mutant embryos (Figure 8G). Taken together, we suspected that Atrn might play corporately with Alkbh4 to regulate the embryonic epiboly through promoting Actin-NMII interaction to form actomyosin ring in the E-YSL.

To further validate our speculation, we generated two different methylation-deficient *actin* mutants (K84A and K84R), and found that the morphological epiboly defects seen in MZ*atrn* mutant embryos could be better rescued by either of these two mutant mRNAs than the wild-type mRNA (Figure 8H and 8I). Combined with our existing data that Atrn interacts with Alkbh4 and increases the binding affinity between Actin and NMII, we demonstrated that Atrn functions together with Alkbh4 to regulate the demethylation of Actin, and subsequently the actomyosin formation.

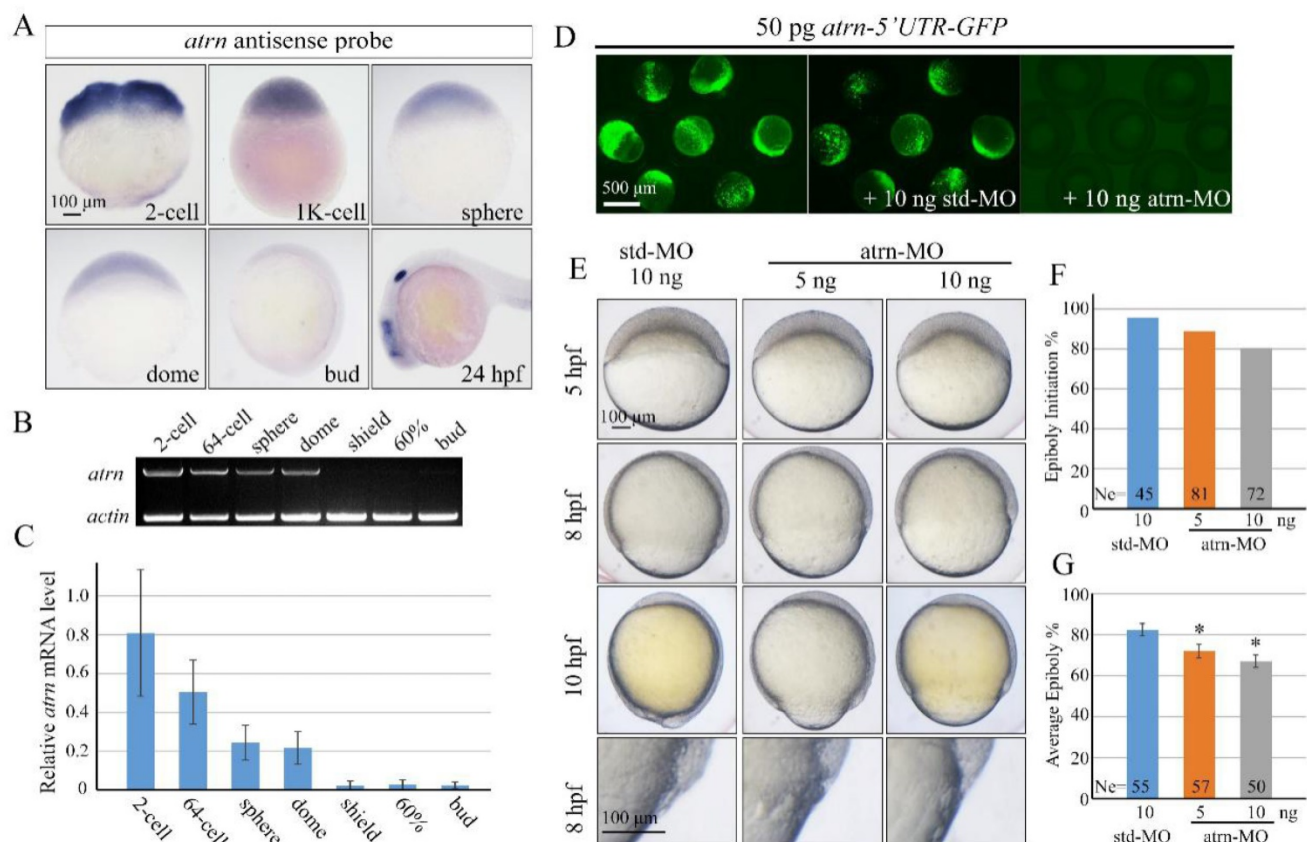


Figure 6. Morpholino knockdown of *atrn* leads to epiboly delay. (A) *atrn* mRNA expression pattern in wild-type embryos was detected by whole-mount *in situ* hybridization at indicated stages. (B, C) Semi-quantitative RT-PCR detection of zebrafish *atrn* mRNA level at indicated stages. The relative expression ratio was calculated from the band intensity between *atrn* and β -*actin* (internal control). (D) Effectiveness of *atrn* morpholino. 50 pg *atrn*-5'UTR-GFP plasmid DNA was injected alone or with 10 ng std-MO or *atrn*-MO at 1-cell stage. The injected embryos were observed for GFP expression at late gastrulation stages. (E) Morpholino knockdown of *atrn* results in epiboly delay in a dose dependent manner. Embryos were observed and imaged at indicated stages. Magnified observations of the embryonic marginal cell layers are shown at the last panel. (F, G) The quantitative data of epiboly initiation at 5 hpf and epiboly progression at 8 hpf in (E) are shown. *, $p < 0.01$. Scale bars: 100 μ m in (A, E); 500 μ m in (D).

MZalkbh4;MZatrn double mutants exhibit a similar phenotype as either of the single mutants

To investigate the genetic relationship between *alkbh4* and *atrn*, we examined maternal-zygotic homozygous embryos for both mutations. Firstly, we got zygotic *alkbh4*^{-/-};*atrn*^{-/-} homozygotes by intercrossing *alkbh4*^{+/-};*atrn*^{+/-} heterozygous. With no obvious morphological defects, zygotic *alkbh4*^{-/-};*atrn*^{-/-} homozygous embryos developed normally to adults, thus allowing generating maternal-zygotic MZ*alkbh4*;MZ*atrn* by intercrossing homozygous fish directly. As shown in Figure 9A and 9B, MZ*alkbh4*;MZ*atrn* double mutants exhibited a similar epibolic delay as either of the single mutants. Co-IP assay was performed to test whether knockdown of *alkbh4* and *atrn* at the same time would affect the

Actin-NMII interaction. As our suspected, it was revealed *in vivo* that the Actin-NMII interaction was also disrupted in double knockdown embryos (Figure 9C). Additionally, we stained the embryos with fluorescent labeled phalloidin and anti-NMII antibody, and found that at 75% epiboly, only a relatively thin band of Actin or NMII was detected in the double mutants at the same time point. Even when they developed to the morphologically comparable stage, the staining of Actin and NMII was still distinctly thinner than the wild-type (Figure 9D and 9E). On the other hand, we also demonstrated a delay of the elongation of the marginal EVL cells in the double mutants (Figure 9F). Thus, it is well demonstrated that the formation of actomyosin band was obviously inhibited in *alkbh4* and *atrn* double mutants.

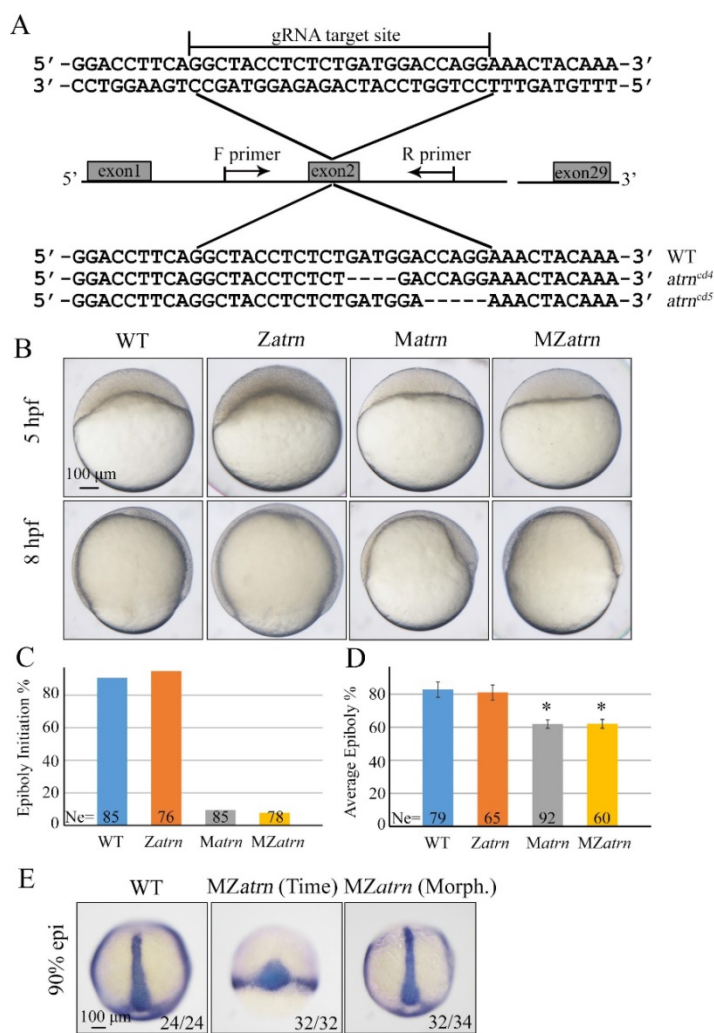


Figure 7. Maternal *atrn* mutation leads to epiboly delay. (A) CRISPR/Cas9-mediated deletion of *atrn*. Zebrafish *atrn* contains 29 exons, and gRNA was designed to target the second exon. Sequencing results of the target sites from several individual F₂ embryos are shown below, including the wild-type form and two *atrn* mutant forms. (B) Maternal but not zygotic *atrn* mutation results in epiboly initiation and progression delays. Wild-type, *Zatrn*, *Matrn* and *MZatrn* mutant embryos were collected after fertilization at the same time and then imaged at indicated time points. (C, D) The quantitative data of epiboly initiation at 5 hpf and epiboly progression at 8 hpf in (B) are shown. (E) CE movements appear essentially normal in *MZatrn* mutant embryos. The mutant embryos were collected at both same time and morphologically comparable stages with wild-type embryos. *dlx3b* and *ntla* probes were used simultaneously for *in situ* hybridization. The ratios of embryos with representative pattern are indicated at the right corner of each picture. *, p<0.01. Scale bars: 100 μm in (B, E).

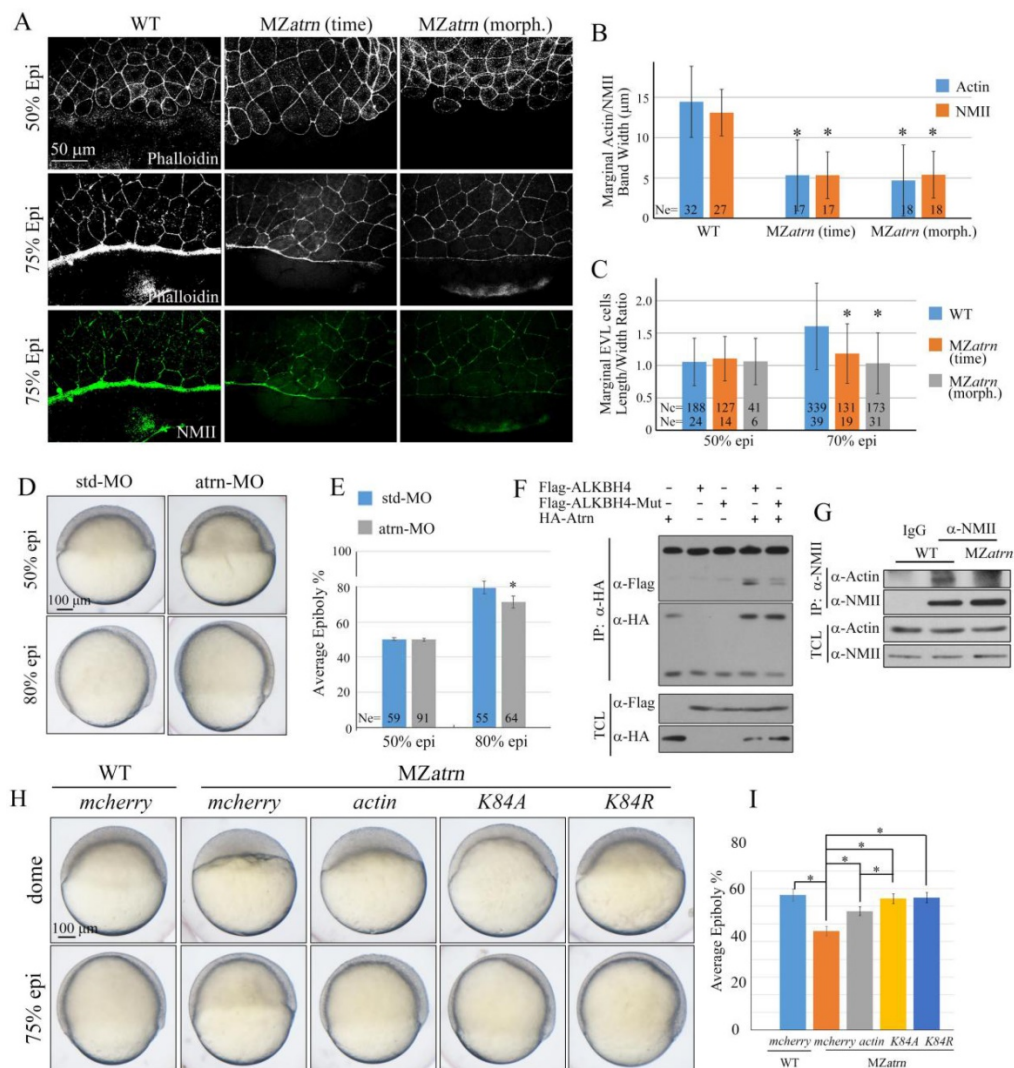


Figure 8. Atrn regulates actomyosin formation and Actin-NMII interaction in zebrafish embryos. (A) Confocal images of phalloidin stained embryos at 50% epiboly, and phalloidin and anti-NMII double stained embryos at 75% epiboly. The mutant embryos were collected at both the same time point and comparable morphological stages compared with wild-type embryos. Embryos were laterally viewed with animal pole to the top and vegetal pole to the bottom. (B) Quantitative measurements of actomyosin band widths in (A) at 75% epiboly stage, which are represented by the widths of Actin and NMII staining in the E-YSL separately. (C) Quantitative measurements of the marginal EVL cell length/width ratios in (A) at both 50% and 75% epiboly stages. Ne, the number of observed embryos; Nc, the number of observed cells. (D) Epiboly defects caused by YSL-injection of atrn-MO. (E) Epiboly progression in (D) was measured by the average epiboly percentage of the embryos. (F) Atrn associated with less catalytically inactive form of ALKBH4 (ALKBH4-Mut), as revealed by co-IP in HEK293T cells. (G) Co-IP assay shows that endogenous Actin-NMII interaction is decreased in MZatrn mutant embryos. Embryos at 75% epiboly were harvested for lysis and Co-IP. (H) Rescue effects of wild-type and two methylation-deficient *actin* mRNAs in MZatrn embryos. 100 pg *mcherry* and different forms of *actin* mRNA were used for injection. Embryos injected with 100 pg *mcherry* mRNA were used as negative controls. Embryos were observed at dome and 75% epiboly stages, and shown as lateral views. (I) Statistical results of (H). *, $p < 0.01$. Scale bars: 50 μm in (A); 100 μm in (D, H).

Discussion

Previous reports indicated that ALKBH4 is essential for the development of spermatocytes by using inducible *Alkbh4* knockout mice, but there is no chance to study the functions of *Alkbh4* in mouse embryonic development due to the lethality of *Alkbh4* homozygous during early preimplantation stage [18]. Here, using zebrafish as animal model, we find that *alkbh4* homozygous mutant embryos can develop to adult normally, which is quite different from the situation in mouse. It is perhaps due to the

redundancy of other *Alkbh* family members or unknown compensatory effects, and thus allowing us to investigate the roles of *Alkbh4* in early development of zebrafish embryos. In this study, we report that maternal mutation of *alkbh4* results in embryonic epiboly delay, aberrant cell shape and impaired actomyosin band formation at the marginal region. Taking into account the facts that *Alkbh4* can demethylate Actin and regulate Actin-NMII interaction, we speculate that *Alkbh4* functions in zebrafish embryonic cell movements by regulating actomyosin band formation in the E-YSL.

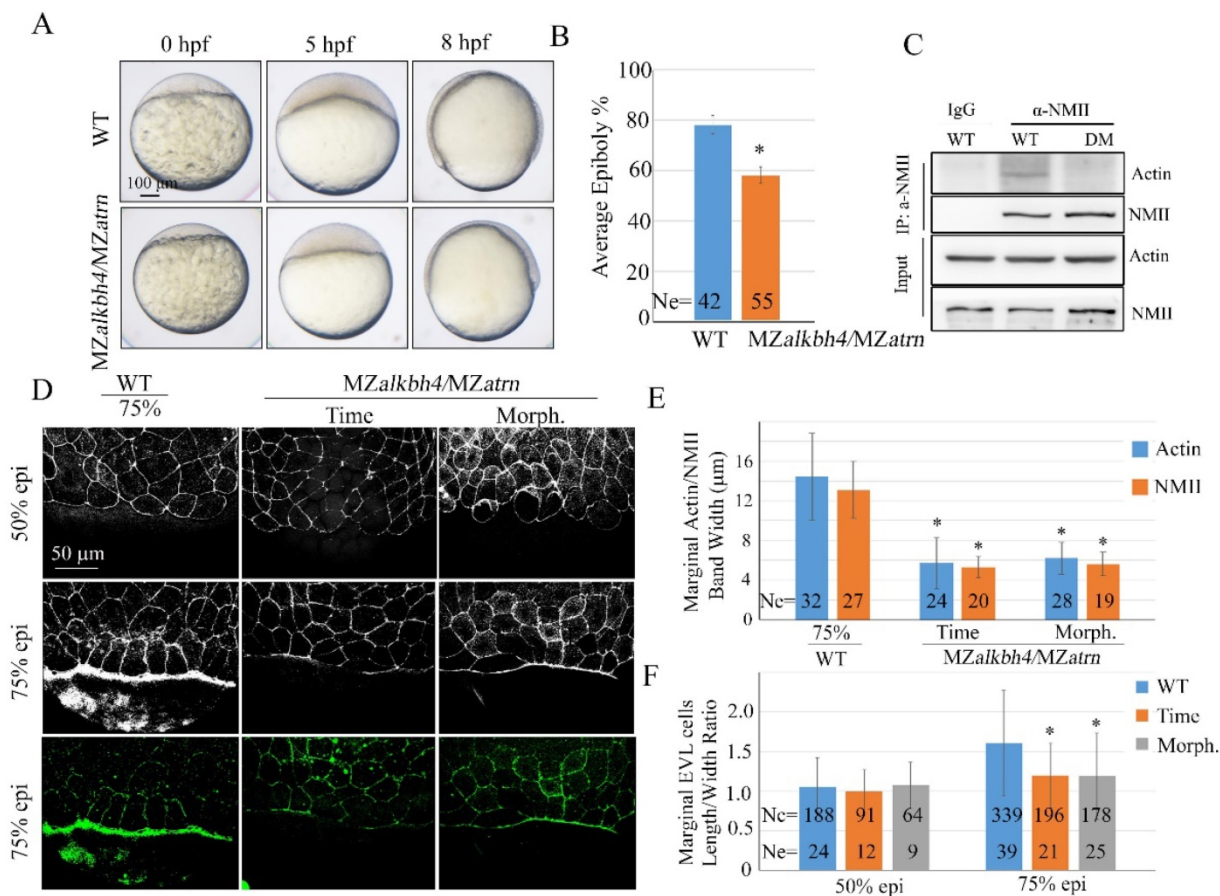


Figure 9. Epiboly and actomyosin formation are defective in MZalkbh4;MZatrn double mutant embryos. (A) Epiboly initiation and progression delay in MZalkbh4;MZatrn double mutants. (B) The quantitative data of epiboly progression at 8 hpf are shown. (C) Co-IP assay shows that endogenous Actin-NMII interaction is decreased in *alkbh4* and *atrn* double morphant embryos. Embryos at 75% epiboly stage were harvested for lysis. (D) Confocal images of phalloidin stained embryos at 50% epiboly, and phalloidin and anti-NMII double stained embryos at 75% epiboly. (E) Quantitative measurements of actomyosin band widths in (D) at 75% epiboly stage. (F) Quantitative measurements of the marginal EVL cell length/width ratios in (D) at both 50% and 75% epiboly stages. Ne, the number of observed embryos; Nc, the number of observed cells. *, $p < 0.01$. Scale bars: 100 µm in (A); 50 µm in (D).

It has been proposed that endocytosis in the E-YSL and longitudinally organized microtubules in the YCL are also regarded as key regulating factors during epiboly progression [5, 37]. Endocytosis in E-YSL is critical for providing a pulling force as the membrane is internalized, and yolk cell microtubules contribute to the vegetal movement of the E-YSN. Here, we found that compared to wild-type embryos, MZalkbh4 and MZatrn mutants internalized Rhodamine-dextran dye in the E-YSL and assembled microtubules in the YCL normally, indicating that they are not the causes of the epiboly defect in our case (Supplementary Figure S3 and S4). Thus, it is believed that Alkbh4 and Atrn regulate embryonic epiboly by promoting Actin-NMII band formation in the E-YSL specifically. Additionally, we also excluded the possibility that the epibolic defects in MZalkbh4 and MZatrn mutants were ascribed to changes in amount of embryonic cells (Supplementary Figure S1) or cell proliferation (Supplementary Figure S5). However, it is noticed that Actin filaments

distribution in cortical yolk cell were severely disrupted in MZalkbh4 mutants, but not in MZatrn mutants as shown in Supplementary Figure S1. As the previous study indicated that the formation of large patches appeared to be devoid of Actin filaments is likely due to the displacement of the cortical cytoplasm by the yolk mass in embryos [36], we speculate that *alkbh4* but not *atrn* might be functional in keeping the integrity of yolk cortical cytoplasmic layer. It will be of great interest to figure out the detailed mechanisms in the future.

Furthermore, we identified Atrn as an Alkbh4 interacting protein, and found that its maternal depletion also causes similar defects in epibolic morphogenesis, as well as the actomyosin band formation during zebrafish early development. Although the molecular mechanisms of Atrn regulating actomyosin formation are not clear until now, our data suggested that Atrn might work together with Alkbh4 to participate in the same process. Based on the fact that Atrn shows a much

lower affinity to interact with catalytically inactive form of Alkbh4, and methylation-deficient *actin* mRNA could rescue the epiboly defects of MZatrn mutant embryos, we speculate that Atrn might be involved in regulating the demethylation activity of Alkbh4. For the underlying mechanisms, there are several other possibilities. Because Atrn protein contains 7 Kelch repeats, which have been implicated in binding to Actin and subsequently regulating the organization of the cytoskeleton, it also can act as a scaffold protein to mediate the interaction between Alkbh4 and Actin, and then promote the actomyosin formation. Besides, we also can't exclude the possibility that Atrn can function in a parallel way to that of Alkbh4 behaves.

As we known, Atrn is most famous as an accessory receptor for Agouti protein in MC1R and MC4R signaling pathway to regulate pigmentation and obesity [38]. In this study, we demonstrate that Atrn plays an important role in modulating actomyosin formation, and subsequently promoting the cell migration in zebrafish embryos for the first time. Actually, MC1R was also reported to play functional role in controlling both human and mouse melanoma cells migration via enhancement of syndecan-2 expression [39]. Whether there is a potential cross talk between Atrn-MC1R and Alkbh4-Atrn signaling need to be investigated further.

In conclusion, results from our studies indicate that Alkbh4 can interact with Atrn, and both genes maternally regulate zebrafish embryonic epiboly via affecting marginal actomyosin band formation. Our studies identified Atrn as a new regulator of actomyosin formation and reflect the importance of maternal genes in early embryonic development.

Supplementary Material

Supplementary figures.

<http://www.ijbs.com/v13p1051s1.pdf>

Acknowledgements

We thank the members of the Meng laboratory for experimental assistance and help discussion. We also thank the Image Core Facility of Protein Technology Center in Tsinghua University. This work was financially supported by grants from the National Natural Science Foundation of China (#31522035, #31371460 and #31590832).

Competing Interests

The authors have declared that no competing interest exists.

References

1. Warga RM, Kimmel CB. Cell movements during epiboly and gastrulation in zebrafish. *Development* 1990; 108: 569-80.
2. Bruce AE. Zebrafish epiboly: Spreading thin over the yolk. *Developmental dynamics: an official publication of the American Association of Anatomists* 2016; 245: 244-58.
3. Zalik SE, Lewandowski E, Kam Z, Geiger B. Cell adhesion and the actin cytoskeleton of the enveloping layer in the zebrafish embryo during epiboly. *Biochemistry and cell biology = Biochimie et biologie cellulaire* 1999; 77: 527-42.
4. Behrndt M, Salbreux G, Campinho P et al. Forces driving epithelial spreading in zebrafish gastrulation. *Science* 2012; 338: 257-60.
5. Cheng JC, Miller AL, Webb SE. Organization and function of microfilaments during late epiboly in zebrafish embryos. *Developmental dynamics: an official publication of the American Association of Anatomists* 2004; 231: 313-23.
6. Koppen M, Fernandez BG, Carvalho L et al. Coordinated cell-shape changes control epithelial movement in zebrafish and *Drosophila*. *Development* 2006; 133: 2671-81.
7. Ougland R, Rognes T, Klungland A, Larsen E. Non-homologous functions of the AlkB homologs. *Journal of molecular cell biology* 2015; 7: 494-504.
8. Duncan T, Trewick SC, Koivisto P et al. Reversal of DNA alkylation damage by two human dioxygenases. *Proceedings of the National Academy of Sciences of the United States of America* 2002; 99: 16660-5.
9. Aas PA, Otterlei M, Falnes PO et al. Human and bacterial oxidative demethylases repair alkylation damage in both RNA and DNA. *Nature* 2003; 421: 859-63.
10. Ringvoll J, Nordstrand LM, Vagbo CB et al. Repair deficient mice reveal mABH2 as the primary oxidative demethylase for repairing 1meA and 3meC lesions in DNA. *The EMBO journal* 2006; 25: 2189-98.
11. Zheng G, Dahl JA, Niu Y et al. ALKBH5 is a mammalian RNA demethylase that impacts RNA metabolism and mouse fertility. *Molecular cell* 2013; 49: 18-29.
12. Jia G, Fu Y, Zhao X et al. N6-methyladenosine in nuclear RNA is a major substrate of the obesity-associated FTO. *Nature chemical biology* 2011; 7: 885-7.
13. Fu D, Brophy JA, Chan CT et al. Human AlkB homolog ABH8 is a tRNA methyltransferase required for wobble uridine modification and DNA damage survival. *Molecular and cellular biology* 2010; 30: 2449-59.
14. Songe-Moller L, van den Born E, Leihne V et al. Mammalian ALKBH8 possesses tRNA methyltransferase activity required for the biogenesis of multiple wobble uridine modifications implicated in translational decoding. *Molecular and cellular biology* 2010; 30: 1814-27.
15. Zdzalik D, Vagbo CB, Kirpekar F et al. Protozoan ALKBH8 oxygenases display both DNA repair and tRNA modification activities. *PLoS one* 2014; 9: e98729.
16. Ougland R, Lando D, Jonson I et al. ALKBH1 is a histone H2A dioxygenase involved in neural differentiation. *Stem cells* 2012; 30: 2672-82.
17. Li MM, Nilsen A, Shi Y et al. ALKBH4-dependent demethylation of actin regulates actomyosin dynamics. *Nature communications* 2013; 4: 1832.
18. Nilsen A, Fusser M, Greggains G et al. ALKBH4 depletion in mice leads to spermatogenic defects. *PLoS one* 2014; 9: e105113.
19. Duke-Cohan JS, Gu J, McLaughlin DF et al. Attractin (DPPT-L), a member of the CUB family of cell adhesion and guidance proteins, is secreted by activated human T lymphocytes and modulates immune cell interactions. *Proceedings of the National Academy of Sciences of the United States of America* 1998; 95: 11336-41.
20. Tang W, Gunn TM, McLaughlin DF et al. Secreted and membrane attractin result from alternative splicing of the human ATRN gene. *Proceedings of the National Academy of Sciences of the United States of America* 2000; 97: 6025-30.
21. Kuramoto T, Nomoto T, Fujiwara A et al. Insertional mutation of the Attractin gene in the black tremor hamster. *Mammalian genome: official journal of the International Mammalian Genome Society* 2002; 13: 36-40.
22. Khwaja FW, Duke-Cohan JS, Brat DJ, Van Meir EG. Attractin is elevated in the cerebrospinal fluid of patients with malignant astrocytoma and mediates glioma cell migration. *Clinical cancer research: an official journal of the American Association for Cancer Research* 2006; 12: 6331-6.
23. Gunn TM, Miller KA, He L et al. The mouse mahogany locus encodes a transmembrane form of human attractin. *Nature* 1999; 398: 152-6.
24. Hida T, Wakamatsu K, Sviderskaya EV et al. Agouti protein, mahogunin, and attractin in pheomelanogenesis and melanoblast-like alteration of melanocytes: a cAMP-independent pathway. *Pigment cell & melanoma research* 2009; 22: 623-34.
25. Paz J, Yao H, Lim HS et al. The neuroprotective role of attractin in neurodegeneration. *Neurobiology of aging* 2007; 28: 1446-56.
26. Tang W, Duke-Cohan JS. Human secreted attractin disrupts neurite formation in differentiating cortical neural cells in vitro. *Journal of neuropathology and experimental neurology* 2002; 61: 767-77.
27. Wrenger S, Faust J, Friedrich D et al. Attractin, a dipeptidyl peptidase IV/CD26-like enzyme, is expressed on human peripheral blood monocytes and potentially influences monocyte function. *Journal of leukocyte biology* 2006; 80: 621-9.
28. He L, Gunn TM, Bouley DM et al. A biochemical function for attractin in agouti-induced pigmentation and obesity. *Nature genetics* 2001; 27: 40-7.
29. Overton JD, Leibel RL. Mahogonoid and mahogany mutations rectify the obesity of the yellow mouse by effects on endosomal traffic of MC4R protein. *The Journal of biological chemistry* 2011; 286: 18914-29.

30. Kimmel CB, Ballard WW, Kimmel SR et al. Stages of embryonic development of the zebrafish. *Developmental dynamics: an official publication of the American Association of Anatomists* 1995; 203: 253-310.
31. Huang H, Lu FI, Jia S et al. Amotl2 is essential for cell movements in zebrafish embryo and regulates c-Src translocation. *Development* 2007; 134: 979-88.
32. Liu X, Xiong C, Jia S et al. Araf kinase antagonizes Nodal-Smad2 activity in mesendoderm development by directly phosphorylating the Smad2 linker region. *Nature communications* 2013; 4: 1728.
33. Zhang Y, Li X, Qi J et al. Rock2 controls TGFbeta signaling and inhibits mesoderm induction in zebrafish embryos. *Journal of cell science* 2009; 122: 2197-207.
34. Abrams EW, Mullins MC. Early zebrafish development: it's in the maternal genes. *Current opinion in genetics & development* 2009; 19: 396-403.
35. Hwang WY, Fu Y, Reyon D et al. Efficient genome editing in zebrafish using a CRISPR-Cas system. *Nature biotechnology* 2013; 31: 227-9.
36. Lachnit M, Kur E, Driever W. Alterations of the cytoskeleton in all three embryonic lineages contribute to the epiboly defect of Pou5f1/Oct4 deficient MZspg zebrafish embryos. *Developmental biology* 2008; 315: 1-17.
37. Solnica-Krezel L, Driever W. Microtubule arrays of the zebrafish yolk cell: organization and function during epiboly. *Development* 1994; 120: 2443-55.
38. Barsh GS, He L, Gunn TM. Genetic and biochemical studies of the Agouti-attractin system. *Journal of receptor and signal transduction research* 2002; 22: 63-77.
39. Chung H, Lee JH, Jeong D et al. Melanocortin 1 receptor regulates melanoma cell migration by controlling syndecan-2 expression. *The Journal of biological chemistry* 2012; 287: 19326-35.